PCCP

PAPER

Cite this: *Phys. Chem. Chem. Phys.*, 2016, **18**, 4585

Efficient microfluidic photocatalysis in a symmetrical metal-cladding waveguide

Shu Zhu, Hailang Dai, Bei Jiang, Zhenhua Shen and Xianfeng Chen*

Received 7th November 2015,
Accepted 28th December 2015

DOI: 10.1039/c5cp06813d

www.rsc.org/pccp

In this paper, a symmetrical metal-cladding optical waveguide based microfluidic chip with a self-organized and free-standing TiO_2 nanotube membrane was utilized to perform efficient photocatalysis. The chip has a microchannel bonded with TiO_2 nanotube coated glass. The employment of microfluidic chip for hydrolysis reaction can enable the transfer of mass and photons. Moreover, the incorporation of the double metal-cladding waveguide enhances the light–matter interaction and effectively improves the efficiency of photocatalysis.

Introduction

With the rapid development of science and technology, profound changes have taken place in urban and rural areas. The demand and calls for curbing environmental pollution, enhancing the quality of life and the construction of an ecological civilization city are increasing. In particular, environmental pollution is still quite serious on the whole, although the situation has improved in some areas after long-term treatments. Currently, to improve the efficiency of environmental pollution control, more and more people have focused their eyes on using a variety of photocatalytic technology to deal with environmental pollution. Photocatalytic technology employs solar energy for the conversion and utilization of energy, mechanistic organic photochemistry, and environmental cleaning. Many physical, chemical and environmental researchers have taken part in these aspects of study with the purpose of solving the obstacles of energy and the environment.[1] As a common material used for photocatalysis, nano-TiO_2 attracts a lot of attention due to its strong ability for oxidation, good stability, low cost and less contamination.[2–5]

The studies reported on photocatalytic reactions are usually carried out in a conventional batch reactor. The reaction volume usually ranges from a few millimeters to several tens millimeters, thus producing a lower reaction efficiency. In recent years, a type of photochemical reaction based on a continuous flow microreactor called as microfluidic technology has been extensively studied. Microfluidic technology, as one of the most cutting-edge fields of science and technology, shows tremendous prospects in bioscience, industrial synthesis and some other fields by virtue of its unique advantages such as good controllability, high-throughput and low-cost.[6] In addition, the microchannel in the chip has a very high specific surface area,[7] which makes the photon and mass transfer efficient during the photoreaction. Thus, the efficiency of photocatalysis would be several times higher than that found in a conventional batch reaction.[7–11]

A reactor based on a TiO_2-coated silica waveguide in an attenuated total reflection (ATR) mode used for the photocatalytic oxidation of formic acid in water has been proposed in 1999.[12] This method could utilize light power more efficiently or enhance the quantum efficiency.[13] During the ATR propagation, incidental light on the interface of silica/TiO_2/water is completely reflected back onto the silica. In every process of reflection, the TiO_2 film absorbs more energy of the UV light. Further improvement in the photocatalytic efficiency remains an important issue and has attracted a lot of attention.

When the incidental light couples onto the guiding layer at the couple angle,[14] more than 1000 ATR modes (ATRM) can be excited in the symmetrical metal-cladding waveguide (SMCW).[15] Due to the strong optical energy confinement of the SMCW, a quality factor of (10^5)[16,17] can be reached. Thus, the incidental light can obtain a gratifying efficiency with high power density. In addition, the SMCW was also highly-sensitive to the incidental wavelength. Herein, we propose a novel microfluidic chip based on the SMCW to enhance the efficiency of photocatalysis. To demonstrate the feasibility of the device, methylene blue was selected as a model for organic wastewater. We also developed a model using finite-difference time-domain (FDTD) to simulate exemplarily a setup to permit an estimation of the increase in light intensity found in the microfluidic chip due to the presence of the SMCW.

State Key Laboratory of Advanced Optical Communication Systems and Networks, Department of Physics and Astronomy, Shanghai Jiao Tong University, 800 Dongchuan Road, Shanghai 200240, China.
E-mail: xfchen@sjtu.edu.cn

Experimental

Fabrication of microfluidic chip based on SMCW

The chip structure is shown in Fig. 1. The microchannel in the microfluidic chip was fabricated using conventional soft lithography techniques. The dimensions of the main channel area are 7 mm in length, 2.5 mm in width and 125 μm in height. Due to the high reflectivity in the UV region, we chose aluminium as the metal-cladding layer. Aluminum film with a thickness of 20 nm was deposited on the top of the main channel area of the PDMS slab for better coupling. Aluminium film with a thickness of 300 nm was deposited on the bottom of the glass slab to prevent light leakage. Then, the PDMS slab with the membrane in its channel and a glass slide were placed into the plasma chamber and exposed to oxygen plasma for permanent bonding. For comparison, a microfluidic chip without the SMCW was also fabricated in this study.

Preparation and characterization of TiO_2 nanotube membrane

The method used to prepare the TiO_2 nanotube membrane is discussed in our previous study.[18] In conclusion, the TiO_2 nanotube membrane was obtained by an anodic oxidation method. The Ti foils act as the working electrode and the Pt acts as the counter electrode. The Ti substrate was first treated in the electrolyte comprised 3 vol% ethylene glycol; deionized water and 0.5 wt% ammonium fluoride at a working voltage of 60 V at room temperature for 1 h, and then a surface layer of TiO_2 can be formed. After removal of the surface TiO_2, the substrate was treated with a second anodization for about 60 minutes at the same working voltage. Finally, the TiO_2 membrane was detached from the substrate after annealing in a furnace at 450 °C for 2 h. Then, the sample was subjected to scanning electron microscopy (SEM, NOVA Nano-SEM230, FEI) for morphological analysis.

Photocatalytic degradation of methylene blue

The effect of the photocatalytic degradation was evaluated using methylene blue (MB) as a model pollutant under the irradiation of a UV lamp. The reaction equation was as follows:

$$2C_6H_{18}N_3SCl + 31O_2 \xrightarrow{TiO_2, h\nu} 2HCl + 2H_2SO_4 + 6HNO_3 + 12CO_2 + 12H_2O \quad (1)$$

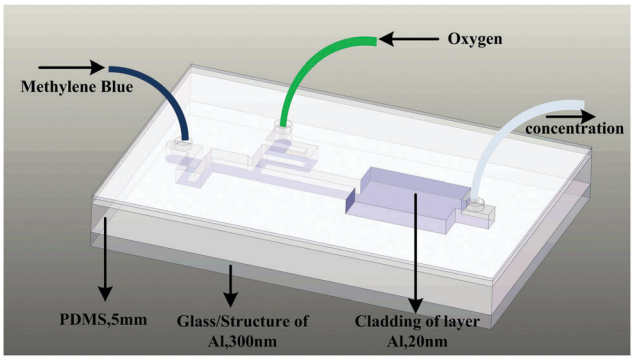

Fig. 1 Diagram of the microfluidic chip based on a symmetrical metal-cladding waveguide.

The initial concentration of MB was about 0.15 g L^{-1} when the precise value was detected using the ATR indicatrix. In a typical experiment, 5 mL of the abovementioned MB solution was injected through the inlet into the microfluidic chip using a syringe pump *via* tygon tubing and oxygen was injected through another inlet at a flow rate of 5 μL min^{-1}.

Results and discussion

Simulation results

To verify the feasibility of the experiment, we built a model, as shown in Fig. 2. A 20 nm aluminum film with an area of 7×2.5 mm^2 was used as the top cladding of the waveguide. The layer underneath was a microchannel with a thickness of 125 μm, which was filled with the MB solution. At the bottom of the microchannel, there was a piece of TiO_2 nanotube membrane with a thickness of 15 μm. Then, another 300 nm thick aluminium film was added as the bottom cladding. The refractive index of the solvent was 1.33 and the dielectric constant of TiO_2 was set at 2.6. Based on the simulation, over 1000 modes can be obtained. The result of the simulation show the optical power intensity distribution of the ultrahigh order modes inside the microchannel based on a symmetrical metal-cladding waveguide, as shown in Fig. 3. The simulation results reveal one of the optical oscillating modes when the incidental light wavelength was 269.4 nm at an incident angle of 43.8°. Because the UV light source was focused using a convex lens in our experiment, the light was coupled into the waveguide through various incident angles, and thus a large portion of the ultra-violet spectrum of sunlight with phonon energies above the bandgap of TiO_2 can be efficiently coupled into the SMCWs under irradiation with ambient sunlight.

Characterization

Fig. 4 shows the SEM image of the annealed free-standing TiO_2 nanotube membrane. The top view of the membrane is shown in Fig. 4(a). The inner diameter of the nanotube is around 80 nm and the thickness of the nanotube is about 10 nm. Fig. 4(b) and (c) show the cross-section of the TiO_2 nanotube membrane with tube lengths of approximately 15 μm.

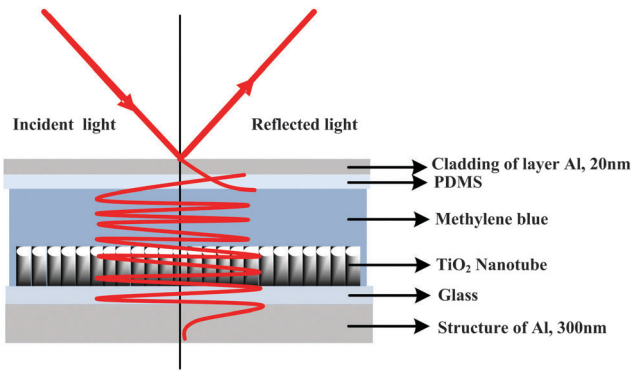

Fig. 2 Schematic diagram of the light coupling process in the symmetrical metal-cladding waveguide used in the photocatalytic degradation of MB.

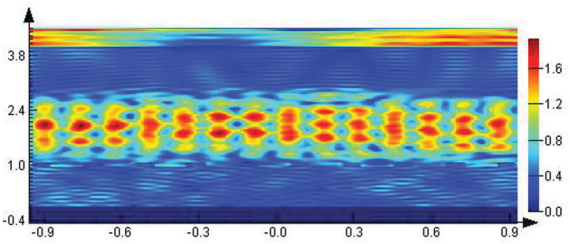

Fig. 3 FDTD simulation results of the increasing light intensity in the waveguide when used in the photocatalytic degradation of MB.

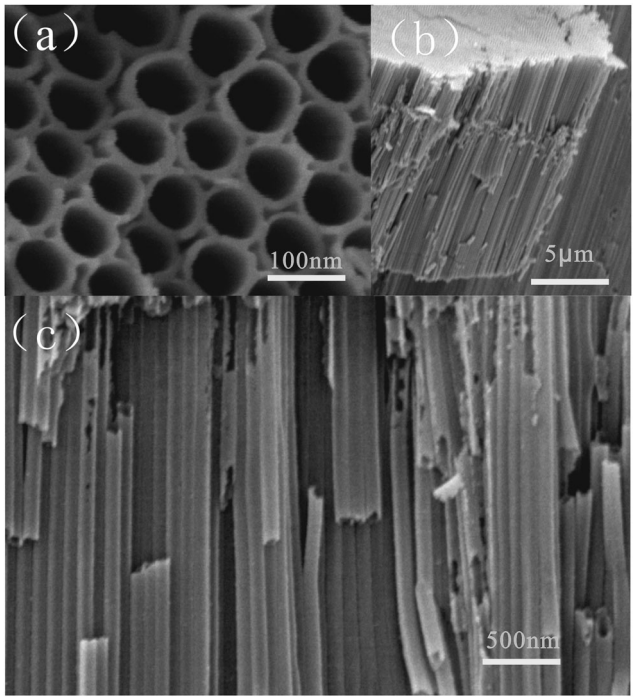

Fig. 4 SEM images of the TiO_2 nanotube membrane. (a) The top view of the nanotubes. (b) The cross-section of the TiO_2 nanotube membrane. (c) The magnified image of the cross-section of the nanotube.

The action principle of SMCW[19,20]

According to the electromagnetic field boundary conditions, the reflectivity can be expressed as follows:

$$R_{\min} = |r_{12}|^2 \left[1 - \frac{4\mathrm{Im}(\beta^0)\mathrm{Im}(\Delta\beta^{\mathrm{rad}})}{(\mathrm{Im}(\beta^0) + \mathrm{Im}(\Delta\beta^{\mathrm{rad}}))^2}\right] \quad (2)$$

$$\beta^0 = k_0 N = k_0 n_0 \sin\theta \quad (3)$$

$$k_0 = 2\pi/\lambda \quad (4)$$

where $\mathrm{Im}(\beta^0)$ and $\mathrm{Im}(\Delta\beta^{\mathrm{rad}})$ are the intrinsic and radiative loss, respectively. β^0 is the propagation constant for an effective index N in the guided modes.

$\mathrm{Im}(\beta^0)$ represents the transmission loss, which is correlated with the extinction coefficient of the waveguide. $\mathrm{Im}(\Delta\beta^{\mathrm{rad}})$ stands for the radiative loss of the guided wave, which is highly associated with the thickness of the metal layer. κ_0 is the wavenumber of light with wavelength λ in free space and θ is the incident angle. When $\mathrm{Im}(\beta^0) = \mathrm{Im}(\Delta\beta^{\mathrm{rad}})$, $R_{\min}$ becomes zero and the critical condition can be realized. Two methods can be applied to figure out the refractive index of the liquid guiding layer inside the symmetric metal cladding waveguide. One is to determine the real part of the complex refractive index of the analyte and the other is to determine the imaginary part of the complex refractive index. The variation in analyte concentration results in a change in the refractive index of the solution, which also affects the resonance angle and the position of ATR tips. In addition, the depth of the dip will rise or fall according to the imaginary part of the complex refractive index. Whether the depth rises or falls relies on the discrepancy between the intrinsic and radiative damping.

Photocatalytic degradation performance of the microfluidic chip

The results of the degradation at a flow rate of 5 μL min^{-1} under the irradiation of an UV lamp were obtained using ATR, as shown in Fig. 5. Fig. 5(a) shows the depth of the dip as the coupled angle decreases from 1.5° to 3.5°. There are black, red and blue curves, representing the initial, with waveguide and without waveguide method, respectively. Fig. 5(b) shows the minimum reflectivity and the concentration of MB, where the incident angle is between 2.25° and 2.40°. As is well known,

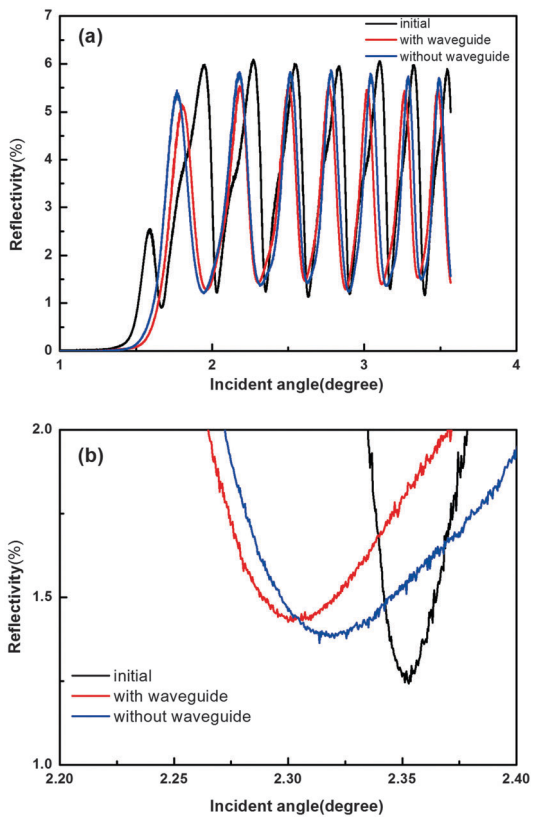

Fig. 5 ATR spectra for the initial MB solution and the photocatalyzed MB solution in the different microfluidic chips. (a) The depth of the dip at the coupled angle decreases from 1.5° to 3.5°. (b) The magnified region of the minimum reflectivity as a function of the concentration of MB, where the incident angle ranges from 2.25° to 2.40°.

Table 1 The concentration of the initial MB solution and photocatalyzed MB solution in the different microfluidic chips

Sample	Concentration (g L^{-1})
Initial	0.143
Without waveguide	0.053
With waveguide	0.017

the higher the concentration is, the higher the intrinsic loss is. Moreover, *via* eqn (2), the higher the intrinsic loss was, the smaller the minimum reflectivity was. In conclusion, the effect of the photocatalysis in the microfluidic chip with SMCW was the best.

Selecting five sets of data from the concentration and minimum reflectivity using the continuous peaks in Fig. 5(a) curve, a set of data was input to calculate the refractive index using software to find the refractive index at different concentrations. We can achieve the relationship between the refractive index and solution concentration using a mathematical expression. Table 1 shows the concentration of initial MB solution and photocatalyzed MB solution in the different microfluidic chips. The original concentration of MB solution was 0.143 g L^{-1}. The concentration of MB solution becomes 0.053 g L^{-1} after the traditional microfluidic photocatalysis process. The efficiency of the photocatalysis was increased by 40% with the help of SMCW and the final concentration was 0.017 g L^{-1} under the same flow rates in the microchannel.

Conclusions

In conclusion, a microfluidic chip based on a SMCW was proposed to realize efficient photocatalysis. The chip was manufactured using a conventional soft lithography technique. The light intensity was largely enhanced due to the excitation of several oscillating modes in the SMCW. As compared with the traditional microfluidic photocatalysis, the symmetrical metal-cladding waveguide based microfluidic photocatalysis demonstrated an increased efficiency of about 40%. The symmetrical metal-cladding waveguide based microfluidic chip offers a great potential platform for efficient wastewater treatment.

Acknowledgements

This study was supported by the National Basic Research Program of China (No. 2011CB808101), the National Natural Science Foundation of China (No. 61125503), the National Basic Research Program of China (No. 2013CBA01703) and the Foundation for the Development of Science and Technology of Shanghai (No. 13JC1408300).

Notes and references

1 M. N. Chong, B. Jin, C. W. Chow and C. Saint, *Water Res.*, 2010, **44**, 2997–3027.
2 V. Shapovalov, *Glass Phys. Chem.*, 2010, **36**, 121–157.
3 J. M. Meichtry, H. J. Lin, L. de la Fuente, I. K. Levy, E. A. Gautier, M. A. Blesa and M. I. Litter, *J. Sol. Energy Eng.*, 2007, **129**, 119–126.
4 M. Ni, M. K. Leung, D. Y. Leung and K. Sumathy, *Renewable Sustainable Energy Rev.*, 2007, **11**, 401–425.
5 X. Zheng, D. Li, X. Li, L. Yu, P. Wang, X. Zhang, J. Fang, Y. Shao and Y. Zheng, *Phys. Chem. Chem. Phys.*, 2014, **16**, 15299–15306.
6 D. Beebe, M. Wheeler, H. Zeringue, E. Walters and S. Raty, *Theriogenology*, 2002, **57**, 125–135.
7 G. Takei, T. Kitamori and H.-B. Kim, *Catal. Commun.*, 2005, **6**, 357–360.
8 H. Lu, M. A. Schmidt and K. F. Jensen, *Lab Chip*, 2001, **1**, 22–28.
9 R. C. Wootton, R. Fortt and A. J. de Mello, *Org. Process Res. Dev.*, 2002, **6**, 187–189.
10 H. Lindstrom, R. Wootton and A. Iles, *AIChE J.*, 2007, **53**, 695–702.
11 R. Gorges, S. Meyer and G. Kreisel, *J. Photochem. Photobiol., A*, 2004, **167**, 95–99.
12 A. L. Lawrence, K. M. McAloon, R. P. Mason and L. M. Mayer, *Environ. Sci. Technol.*, 1999, **33**, 1871–1876.
13 T. Xu, L. Huang, D. Wei, Y. Jin, J. Fang, G. Yuan, Z. Cao and H. Li, *Opt. Commun.*, 2014, **333**, 67–70.
14 W. Yuan, C. Yin, H. Li, P. Xiao and Z. Cao, *J. Opt. Soc. Am. B*, 2011, **28**, 968–971.
15 J. Sun, C. Yin, C. Zhu, X. Wang, W. Yuan, P. Xiao, X. Chen and Z. Cao, *J. Opt. Soc. Am. B*, 2012, **29**, 769–773.
16 X. Wang, C. Yin, H. Li, M. Sang, W. Yuan and Z. Cao, *Opt. Lett.*, 2013, **38**, 4085–4087.
17 L. Xiang, C. Zhuang-Qi, S. Qi-Shun, M. Qing-Hua, H. De-Ying, G. Kun-Peng, Q. Ling and S. Yu-Quan, *Chin. Phys. Lett.*, 2006, **23**, 998.
18 S. Zhu, X. Liu, J. Lin and X. Chen, *Opt. Mater. Express*, 2015, **5**, 2754–2760.
19 H. Dai, M. Sang, Y. Wang, R. Du, W. Yuan, Z. Jia, Z. Cao and X. Chen, *Sens. Actuators, A*, 2014, **218**, 88–93.
20 H. Li, Z. Cao, H. Lu and Q. Shen, *Appl. Phys. Lett.*, 2003, **83**, 2757–2759.

